# A multi-wing chaotic attractor generated via Julia fractal process in a new 3D chaotic system

M. I. KOPP[1], I. SAMUILIK[2,3]
[1]Institute for Single Crystals, NAS UKRAINE, Nauky Ave. 60,
Kharkiv 61072,
UKRAINE

[2]Institute of Life Sciences and Technologies, Daugavpils University,
13 Vienibas Street, LV-5401 Daugavpils,
LATVIA

[3]Institute of Applied Mathematics, Riga Technical University,
LV-1048 Riga,
LATVIA

*Abstract:* This paper introduces a novel three-dimensional chaotic system with minimal algebraic complexity, combining hyperbolic tangent and absolute value nonlinearities in only five terms. Despite its structural simplicity, the system exhibits rich chaotic dynamics verified by positive Lyapunov exponents and fractional Kaplan-Yorke dimension. By applying Julia fractal transformations to the system's state variables, we generate complex multi-wing chaotic attractors with controllable structure and enhanced topological complexity. The number of wings is directly determined by the polynomial order $m$, enabling systematic generation of multi-wing configurations. The scaling coefficient $k$ controls spatial extent, while the complex constant $Z_0$ modulates wing symmetry and distribution. The fractal transformation preserves dissipative and chaotic properties while enriching phase space geometry through smooth, analytically defined polynomial mappings. Potential applications include secure communication, chaotic encryption, random number generation, and biomedical signal processing.

*Key-Words:* chaotic system, hyperbolic tangent, absolute nonlinearity, Julia fractal, multi-wing attractor

Received: September 13, 2025. Revised: April 16, 2026. Accepted: May 9, 2026. Published: July 17, 2026.

## 1 Introduction

Three-dimensional chaotic systems represent a fundamental class of nonlinear dynamical systems capable of demonstrating complex aperiodic behavior with relatively simple mathematical structure. The systematic study of three-dimensional chaos was initiated by the classical works of Lorenz [1], Rössler [2], and Chua [3], which demonstrated that deterministic systems with a minimal number of variables can generate unpredictable dynamics. Since these pioneering studies, numerous variations of three-dimensional chaotic systems with different types of nonlinearities have been proposed.

An extensive comparative analysis of fifty three-dimensional chaotic systems was presented in [4], where the main characteristics of known models, including their topological properties, Lyapunov exponents, and practical applications, were systematized. Remarkably, among the systems considered, only two models utilized absolute value nonlinearity, while systems with hyperbolic tangent nonlinearity were not represented in this review at all. Meanwhile, the choice of nonlinearity type significantly affects the dynamic properties of the system and the possibilities for its practical implementation. Systems with absolute nonlinearity attract particular attention due to the simplicity of circuit implementation, since they do not require analog multipliers, and possess a number of unique properties, such as hidden attractors, multistability, and the ability to shift the attractor without changing the dynamics.

In recent years, there has been a significant increase in interest in three-dimensional systems with absolute nonlinearity. Thus, in [5], a new three-dimensional chaotic system with line equilibrium was proposed, possessing hidden attractors and demonstrating high efficiency in image encryption tasks. A system with variable boosting and hidden attractors was investigated in [6], where the possibility of controlling the position of the attractor in phase space was shown. Further development of this direction is presented in [7], where systems with a single absolute term are proposed, demonstrating rich dynamics and promising applications in data encryption. Of particular interest is the recently published work [8], which presents a new three-dimensional chaotic model of financial processes with absolute nonlinearity. This system is characterized by a maximal Lyapunov exponent of $0.1355$, demonstrating multistability with coexistence of chaotic and periodic attractors. A system with an extremely wide offset range was analyzed in [9], which expands the possibilities for synchronization control. Parallel to systems using absolute nonlinearity, research on three-dimensional chaotic systems with the hyperbolic tangent function tanh($x$) is actively developing. This function has a number of advantages: it is smooth, bounded (with values in the interval $(-1, 1)$), and monotonically increasing, which simplifies mathematical analysis compared to piecewise linear functions. Systems with tanh-nonlinearity are often used to replace piecewise linear characteristics, for example, in Chua's circuit, while ensuring continuous differentiability, which significantly simplifies the calculation of Lyapunov exponents and Jacobians.

In [10], three-dimensional jerk systems with a single tanh-nonlinearity are investigated, characterized by a third-order differential equation of the form $\dddot{x} = J(\ddot{x}, \dot{x}, x)$, where the function $J$ contains a hyperbolic tangent term. It was shown that such systems can be implemented as compact electrical circuits and find applications in biomedical modeling. Modifications of classical Lorenz and cubic systems by introducing tanh-terms allow the generation of different types of attractors: single scrolls when the term is introduced in the third state, double scrolls in the first state, and four scrolls in the second state. Systems without equilibrium points possessing tanh-nonlinearity [10] attract particular attention. Such systems demonstrate hidden attractors and are of significant interest for the theory of nonlinear dynamical systems. The generation of multi-scroll attractors through composite hyperbolic tangent functions was investigated in [11], where it was shown that sequences of tanh-functions create "grids" of attractors through multiple switching points in phase space.

An alternative approach to constructing complex attractors was proposed by Elwakil et al. [12], who modified a Lorenz-type system to create an attractor with a complex "butterfly-like" structure. Their work demonstrated that purposeful modification of nonlinear terms can lead to qualitatively new topological forms of attractors. Of particular interest are systems with absolute nonlinearity investigated by Tamba et al. [13], where it was shown that introducing a term of the form $|x|$ into a system of differential equations not only simplifies circuit implementation but also generates rich dynamics, including chaotic regimes with unusual synchronization properties. This work emphasized the promise of using piecewise linear nonlinearities for generating chaotic signals in applications requiring a high degree of unpredictability. Despite significant progress in studying three-dimensional chaotic systems with various types of nonlinearities, the generation of multi-wing attractors remains a relevant problem. Multi-wing attractors possess a more complex topological structure compared to classical double-scroll systems like Lorenz or Chua, which expands the possibilities for their application in secure communication systems, pseudo-random sequence generation, encryption of medical and color images, as well as in modeling complex processes in economics, biology, and electronic circuits.

A promising direction for generating multi-wing attractors is the use of fractal processes. In [14],[15], a method for generating a multi-wing spherical chaotic attractor by embedding a fractal process directly into the differential equations of the system was proposed. This approach leads to a change in the vector field itself and represents a dynamically equivalent transformation in which equilibrium points do not multiply but unfold in space, generating a multi-wing structure. This is a rigorous dynamical transformation preserving the fundamental properties of the original system. An alternative approach is presented in [16],[17], where the Julia fractal process is applied to the trajectories (signals) of a chaotic memristive system through coordinate transformation or iterative mapping. In contrast to the method of embedding the fractal into the vector field, this approach represents fractal design rather than fractal dynamics, providing visual enrichment of the attractor structure without changing the basic dynamics of the system.

In the present work, a new three-dimensional chaotic system is proposed that combines both types of nonlinearities: the absolute function and the hyperbolic tangent. A distinctive feature of the proposed system is its minimal algebraic complexity: it contains only five terms in the right-hand sides of the differential equations, making it one of the simplest among known three-dimensional chaotic systems with combined nonlinearity. Despite its structural simplicity, the system demonstrates rich dynamics and serves as a basis for developing a method for generating multi-wing chaotic attractors through a process based on Julia fractals. The proposed approach allows the purposeful construction of complex attractors with a specified number of wings, opening new prospects for controlling the topology of chaotic systems while maintaining computational efficiency.

The paper is organized as follows. The Introduction provides a brief overview of the current state of the problem. Section 2 presents a mathematical description of the new three-dimensional chaotic system with combined nonlinearity. Section 3 is devoted to dynamical analysis of the proposed system, including investigation of equilibrium points, local stability, and geometric structure of phase portraits. Section 4 describes the method of applying the Julia fractal process to the new three-dimensional chaotic system for generating multi-wing attractors. Section 5 investigates multi-wing chaotic systems obtained

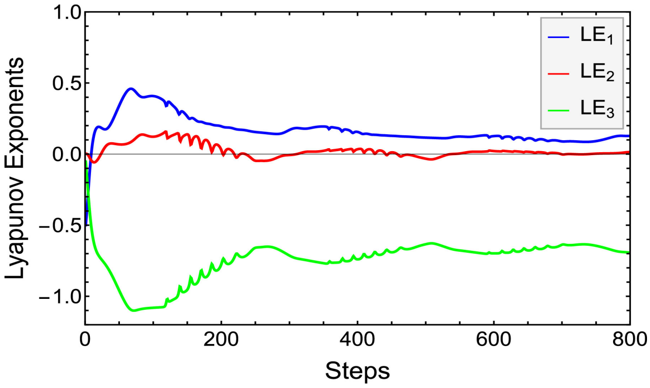


Figure 1: Convergence plot of the Lyapunov exponents for system (1) with $a = 0.55$.

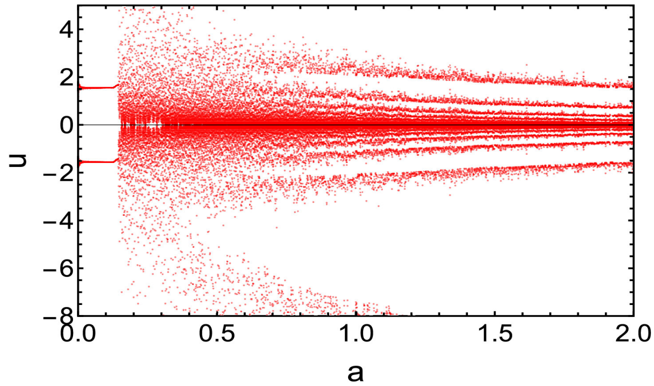


Figure 2: Bifurcation diagram versus parameter $a$.

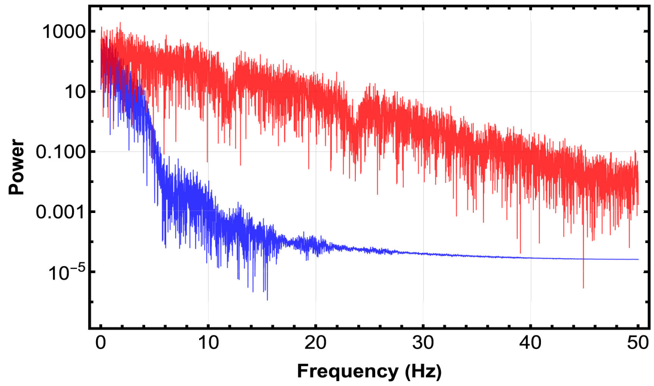


Figure 3: Power spectra of the system (1) (blue) and Lorenz system (red).

through the modified Julia fractal with a scaling coefficient. Section 6 is devoted to the generation of multi-wing chaotic systems using high-order Julia fractals. Section 7 analyzes the influence of a nonzero complex constant on the structure of multi-wing attractors. The Conclusion summarizes the main results of the work and outlines directions for future research.

## 2 A mathematical model of the new proposed 3D dynamic system

In this section, we present a method for deriving a new 3D dynamical system from a modified Lorenz system [12], where the linear piecewise signum function is replaced with the hyperbolic tangent function, as follows:

$$\begin{cases} \dfrac{du}{dt} = a(-u+v) \\ \dfrac{dv}{dt} = -w\tanh u \\ \dfrac{dw}{dt} = |u| - 1 \end{cases} \tag{1}$$

where $a = 0.55$ and the initial conditions are $u(0) = v(0) = w(0) = 1$. Note that the chaotic attractors in system (1) exhibit a different topology compared to those in the standard Lorenz system [1]. In system (1), the chaotic attractors form phase portraits resembling two-winged butterflies. Using the methodology of Binouse et al. [19] and Sandri [20], we can computed all LEs

$$LE_1 = 0.12790, \quad LE_2 \approx 0, \quad LE_3 = -0.69261.$$

Consequently, system (1) exhibits chaotic behavior, as indicated by the presence of a positive Lyapunov exponent. Fig. 1 illustrates the dynamics of the Lyapunov exponents corresponding to chaotic behavior at $a = 0.55$. The corresponding Kaplan-Yorke dimension is approximately $D_{KY} \approx 2.206$, which is notably higher than that of the Lorenz system ($D_{KY} \approx 2.06$) [18]. The bifurcation diagram with respect to variations in the parameter $a$ is depicted in Fig. 2. These results clearly indicate that system (1) exhibits chaotic regimes over an interval $a \in (0.18, 2)$.

Fig. 3 shows the power spectra of system (1) and the Lorenz system [1], shown in blue and red, respectively. The spectrum of system (1) exhibits a sharp power-law decay with energy concentrated in the low-frequency region (0-5 Hz). The nonsmooth nonlinearity $|u|$ generates a complex folded structure of the attractor, resulting in a high fractal dimension despite the compact spectrum. In contrast, the Lorenz system displays a more uniform energy distribution across frequencies with two distinct peaks around 5-10 Hz and 15-20 Hz, reflecting the characteristic switching dynamics between the attractor's lobes. The fully smooth nonlinearities yield lower geometric complexity despite the broader spectral content. These results demonstrate that spectral characteristics do not directly correlate with fractal dimension: nonsmooth systems can exhibit higher Kaplan-Yorke dimensions while maintaining visually simpler frequency spectra.

# 3 Dynamic analysis

In this section, the fundamental dynamical properties of the proposed system (1) are investigated.

## 3.1 Equilibrium points and local stability analysis

System (1) is invariant under the discrete symmetry transformation

$$\mathcal{S}: \ (u, v, w) \mapsto (-u, -v, w). \tag{2}$$

Indeed, under this transformation the right-hand sides of system (1) remain unchanged, since $|u|$ and $\tanh u$ are even and odd functions of $u$, respectively. As a consequence of this symmetry, the phase space is divided into two symmetric regions with respect to the $(w)$-axis, and the system possesses a pair of symmetric equilibrium points

$$E_1 = (1, 1, 0), \qquad E_2 = (-1, -1, 0),$$

which are mapped into each other by $\mathcal{S}$.

A direct substitution confirms that both points satisfy $\dot{u} = \dot{v} = \dot{w} = 0$. The Jacobian matrix of system (1) is given by

$$J(u, v, w) = \begin{pmatrix} -a & a & 0 \\ -w\,\mathrm{sech}^2 u & 0 & -\tanh u \\ \mathrm{sgn}(u) & 0 & 0 \end{pmatrix}. \tag{3}$$

Evaluating the Jacobian at the equilibrium points yields identical characteristic equations for $E_1$ and $E_2$:

$$P(\lambda) \equiv A_0\lambda^3 + A_1\lambda^2 + A_3 = 0, \tag{4}$$

where

$$A_0 = 1, \ A_1 = a, \ A_2 = 0, \ A_3 = a\tanh(1).$$

The system is stable if and only if all principal minors of the Hurwitz determinant are positive [21]:

$$A_0 > 0, \quad \Delta_1 = A_1 > 0, \quad \Delta_2 = A_1A_2 - A_0A_3 > 0. \tag{5}$$

According to the Routh-Hurwitz stability criterion (5) for equation (4) at $a = 0.55$, we find

$$\Delta_1 = 0.55 > 0, \quad \Delta_2 = -0.4188 < 0 \tag{6}$$

Since not all Hurwitz minors are positive, the characteristic equation (4) has roots with positive real parts, indicating instability.

$$\lambda_1 = -0.9833, \qquad \lambda_{2,3} = 0.2166 \pm 0.6157\,\mathrm{i}. \tag{7}$$

Since each equilibrium point has one negative real eigenvalue and a pair of complex conjugate eigenvalues with positive real part, both $E_1$ and $E_2$ are unstable saddle-focus equilibria. The negative real eigenvalue $\lambda_1 = -0.9833$ defines a one-dimensional stable manifold $W^s$: trajectories starting near $E_{1,2}$ along this direction are attracted toward the equilibrium. A pair of complex conjugate eigenvalues $\lambda_{2,3} = 0.2166 \pm 0.6157\,\mathrm{i}$ with positive real parts forms a two-dimensional unstable manifold $W^u$, causing trajectories to spiral away from the equilibrium in the plane spanned by the corresponding eigenvectors. The competition between $W^s$ and $W^u$ generates a Shilnikov-type mechanism: a trajectory is attracted toward $E_1$ along $W^s$, undergoes a spiral motion in $W^u$, and then switches to the neighborhood of $E_2$, repeating the cycle. This explains the characteristic double-wing butterfly-like structure shown in Fig. 4.

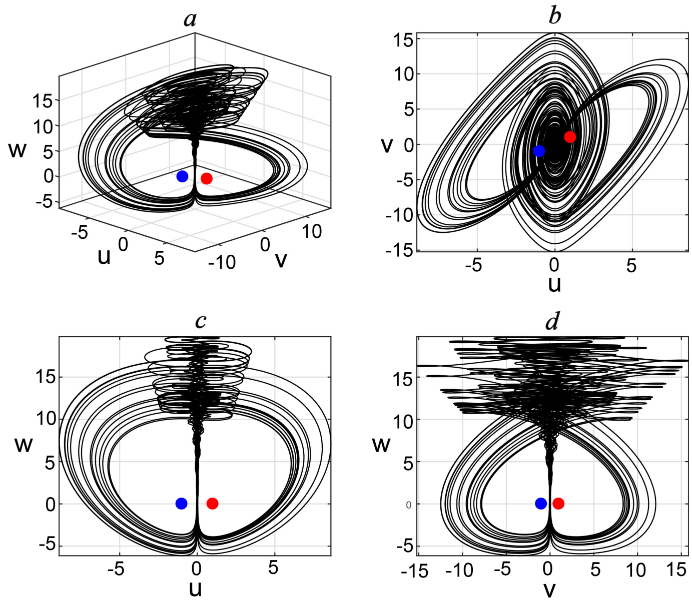


Figure 4: Phase portraits of system (1) for $a = 0.55$: (a) 3D attractor; (b) u-v; (c) u-w; (d) v-w planar projections. Equilibria $E_1$ and $E_2$ are marked by red and blue dots.

The system symmetry $\mathcal{S} : (u, v, w) \mapsto (-u, -v, w)$ ensures that both wings of the attractor are topologically identical and related by this mapping. Unlike the Lorenz attractor, where switching between wings is determined by the sign of variable $x$, switching in system (1) is governed by the sign of $u$ via the $|u|$ nonlinearity in the third equation. This results in a higher fractal dimension and a more compact power spectrum (Fig. 3).

## 3.2 Phase portraits

Figure 4 illustrates the numerical simulation of system (1) in the three-dimensional phase space and its planar projections. The 3D attractor exhibits a two-winged butterfly-like structure, with each wing organized around one of the saddle-focus equilibria $E_1$ and $E_2$. The projections onto the $(u, v)$, $(u, w)$, and $(v, w)$ planes further reveal the spiral nature of trajectories near the equilibria, consistent with the presence of complex eigenvalues. The observed switching of trajectories between the neighborhoods of $E_1$ and $E_2$ is governed by the unstable manifolds and leads to sustained chaotic motion. This mechanism explains the emergence of the double-scroll-type chaotic attractor observed in Fig. 4, while maintaining a topology distinct from the classical Lorenz attractor.

### 3.3 Statistical analysis: 0-1 test for chaos

To provide rigorous statistical confirmation of the chaotic nature of system (1), we apply the 0-1 test for chaos proposed by Gottwald and Melbourne [22, 23]. Unlike the classical Lyapunov exponent analysis, the 0-1 test operates directly on a scalar time series without requiring phase-space reconstruction or knowledge of the underlying equations, and yields a single binary indicator $K \in [0, 1]$: $K \approx 1$ indicates chaotic dynamics, whereas $K \approx 0$ corresponds to regular (periodic or quasi-periodic) behaviour.

Let $\{\varphi(n)\}_{n=1}^{N}$ be a scalar observable extracted from the trajectory of system (1); here we use the variable $u(n)$. For a fixed parameter $c \in (0, 2\pi)$, two auxiliary variables are defined by the cumulative sums

$$p_c(n) = \sum_{j=1}^{n} \varphi(j)\cos(cj), \qquad q_c(n) = \sum_{j=1}^{n} \varphi(j)\sin(cj). \tag{8}$$

The mean square displacement of the vector $(p_c, q_c)$ is then computed as

$$M_c(n) = \lim_{N\to\infty} \frac{1}{N}\sum_{j=1}^{N}\Big[\big(p_c(j+n) - p_c(j)\big)^2 + \big(q_c(j+n) - q_c(j)\big)^2\Big] - V_{\text{osc}}(c, n), \tag{9}$$

where the oscillatory correction term is $V_{\text{osc}}(c, n) = \big(\langle\varphi^2\rangle\,(1 - \cos nc)\big)/(1 - \cos c)$, with $\langle\varphi^2\rangle$ denoting the time average of $\varphi^2$. The asymptotic growth rate of $M_c(n)$ discriminates between the two regimes: for chaotic dynamics $M_c(n)$ grows linearly in $n$ (diffusive behaviour of the $(p_c, q_c)$ trajectory), whereas for regular dynamics $M_c(n)$ remains bounded. The binary indicator is obtained as the correlation coefficient

$$K_c = \text{corr}(\,\mathbf{n},\, \mathbf{M}_c) = \frac{\text{cov}(\mathbf{n},\, \mathbf{M}_c)}{\sqrt{\text{var}(\mathbf{n})\,\text{var}(\mathbf{M}_c)}}, \tag{10}$$

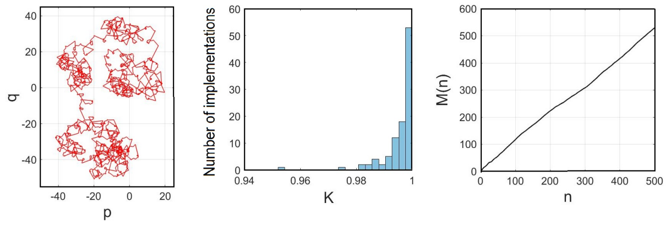


Figure 5: Results of the 0–1 test for chaos for system (1) with $a = 0.55$. Left: unbounded Brownian-like trajectory of $(p_c(n), q_c(n))$, characteristic of chaotic dynamics. Centre: histogram of $K_c$ over $n_c = 100$ values of $c$, sharply concentrated near $K_c \approx 1$. Right: linear growth of $M(n)$ versus $n$, confirming diffusive behaviour. Median $K = 0.9978 \approx 1$ confirms chaos in system (1).

where $\mathbf{n} = (1, 2, \ldots, n_{\max})^\top$ and $\mathbf{M}_c = (M_c(1), \ldots, M_c(n_{\max}))^\top$ with $n_{\max} = \lfloor N/10 \rfloor$. To suppress the sensitivity of $K_c$ to the particular choice of $c$, the final estimate is taken as the median over $n_c = 100$ values of $c$ drawn uniformly from $(\pi/5, 4\pi/5)$, avoiding resonances with dominant frequencies of the signal [22]:

$$K = \text{median}_c\{K_c\}. \tag{11}$$

System (1) was integrated with $a = 0.55$ and initial conditions $(u_0, v_0, w_0) = (1, 1, 1)$ over the interval $t \in [0, 8000]$ using a Runge–Kutta solver with relative tolerance $10^{-9}$. The first 30% of the trajectory was discarded as a transient, and $N = 5000$ uniformly subsampled points of the variable $u(t)$ were used as the observable $\varphi$. The numerical results are summarised as follows:

$$K = \text{median}\{K_c\} = 0.9978, \ \langle K_c\rangle = 0.9955, \quad \sigma_K = 0.0064. \tag{12}$$

The value $K = 0.9978 \approx 1$, obtained from a time series of $N = 5000$ points, unambiguously confirms the chaotic nature of the dynamics of system (1). The small standard deviation $\sigma_K = 0.0064$ demonstrates that the estimate is robust with respect to the choice of the parameter $c$.

The results are illustrated in Fig. 5. The left panel shows the trajectory of the auxiliary vector $(p_c(n),\, q_c(n))$ in the $(p, q)$-plane for a representative value of $c$. The trajectory exhibits unbounded, diffusion-like Brownian motion over the range $p, q \in [-45, 45]$, which is the hallmark of chaotic dynamics; a regular system would produce a bounded Lissajous-type curve. The central panel displays the histogram of $K_c$ values over all $n_c = 100$ realisations of $c$: the distribution is sharply concentrated in the interval $[0.99, 1.00]$ with no values below $0.94$, confirming the robustness of the estimate. The right panel presents the mean square displacement $M(n)$ as a function of $n$: the clearly linear growth with slope approximately equal to unity is consistent with the diffusive regime predicted by theory [22] for chaotic systems, and is in sharp contrast with the bounded $M(n)$ expected for quasi-periodic motion.

# 4 Fractal process in a new 3D chaotic system

To generate multi-scroll chaotic attractors, we apply the classical Julia fractal process to system (1). The Julia set iteration is given by $Z_{n+1} = Z_n^2 + Z_0$, where $Z_n = x_n + iy_n$ are complex numbers. Initially, we set $Z_0 = 0$ to focus on the fundamental transformation. Let $Y = \mathbb{R}^3$ with coordinates $(u, v, w)$. We define the fractal mapping $f : X \to Y$ as [14, 15]:

$$f : (x, y, z) \mapsto (x^2 - y^2, 2xy, z), \qquad (13)$$

or equivalently,

$$u = x^2 - y^2, \quad v = 2xy, \quad w = z. \qquad (14)$$

The Jacobian matrix of this mapping is:

$$Df = \begin{bmatrix} \frac{\partial u}{\partial x} & \frac{\partial u}{\partial y} & \frac{\partial u}{\partial z} \\ \frac{\partial v}{\partial x} & \frac{\partial v}{\partial y} & \frac{\partial v}{\partial z} \\ \frac{\partial w}{\partial x} & \frac{\partial w}{\partial y} & \frac{\partial w}{\partial z} \end{bmatrix} = \begin{bmatrix} 2x & -2y & 0 \\ 2y & 2x & 0 \\ 0 & 0 & 1 \end{bmatrix}. \qquad (15)$$

The inverse Jacobian is:

$$Df^{-1} = \frac{1}{2(x^2+y^2)} \begin{bmatrix} x & y & 0 \\ -y & x & 0 \\ 0 & 0 & 2(x^2+y^2) \end{bmatrix}. \qquad (16)$$

The relationship between the coordinate systems is given by:

$$\begin{bmatrix} \dot{u} \\ \dot{v} \\ \dot{w} \end{bmatrix} = Df \begin{bmatrix} \dot{x} \\ \dot{y} \\ \dot{z} \end{bmatrix}. \qquad (17)$$

Therefore, we obtain:

$$\begin{bmatrix} \dot{x} \\ \dot{y} \\ \dot{z} \end{bmatrix} = Df^{-1} \begin{bmatrix} \dot{u} \\ \dot{v} \\ \dot{w} \end{bmatrix} = \frac{1}{2(x^2+y^2)} \times$$

$$\times \begin{bmatrix} x & y & 0 \\ -y & x & 0 \\ 0 & 0 & 2(x^2+y^2) \end{bmatrix} \begin{bmatrix} \dot{u} \\ \dot{v} \\ \dot{w} \end{bmatrix}. \qquad (18)$$

Substituting $u = x^2 - y^2$, $v = 2xy$, and $w = z$ into system (1), we obtain the transformed system components:

$$\begin{bmatrix} \dot{u} \\ \dot{v} \\ \dot{w} \end{bmatrix} = \begin{bmatrix} a[-(x^2-y^2)+2xy] \\ -z\tanh(x^2-y^2) \\ |x^2-y^2|-1 \end{bmatrix}. \qquad (19)$$

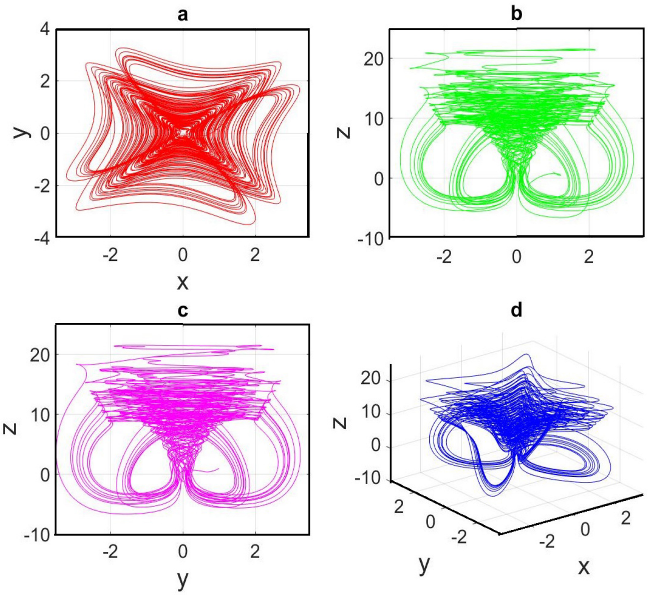


Figure 6: Phase space projections (a)-(c) and 3D portrait (d) of the multi-wing chaotic attractor generated by system (20).

Applying the inverse Jacobian transformation (18) to (19), the multi-wing chaotic system becomes:

$$\begin{cases} \dot{x} = \frac{x}{2(x^2+y^2)}\left[a(-(x^2-y^2)+2xy)\right] + \\ + \frac{y}{2(x^2+y^2)}\left[-z\tanh(x^2-y^2)\right], \\ \dot{y} = \frac{-y}{2(x^2+y^2)}\left[a(-(x^2-y^2)+2xy)\right] + \\ + \frac{x}{2(x^2+y^2)}\left[-z\tanh(x^2-y^2)\right], \\ \dot{z} = |x^2-y^2|-1. \end{cases} \qquad (20)$$

System (20) represents the multi-wing chaotic system obtained by applying the Julia fractal process to the original system (1). This transformation generates a richer chaotic attractor with multiple wins, where the number of wings can be controlled through the fractal process parameters.

The geometric structure of the resulting multi-wing attractor is illustrated in Fig. 6, which presents four complementary perspectives of the phase space dynamics. The $x$-$y$ plane projection reveals a characteristic four-wing butterfly-like structure with pronounced lobes extending symmetrically from the central region. This symmetry is a direct consequence of the quadratic transformation $f$ in equation (13), which maps the original dynamics onto a surface exhibiting rotational symmetry. The vertical projections ($x$-$z$ and $y$-$z$ planes) demonstrate the complex stretching and folding mechanism in the $z$-direction, where the attractor exhibits a funnel-shaped structure expanding from approximately $z = -5$ to $z = 22$.

These projections reveal how trajectories spiral outward in the horizontal plane while simultaneously being stretched vertically, creating multiple layers of orbits that characterize the multi-wing topology. The 3D phase portrait synthesizes these observations, showing how the four wings emerge naturally from the interplay between the horizontal expansion induced by the Julia transformation and the vertical dynamics governed by the absolute value nonlinearity in the $z$-component. The dense concentration of trajectories near the center, gradually dispersing into distinct wing structures, indicates the presence of an unstable equilibrium region from which chaotic orbits are repelled into the outer lobes. This morphology demonstrates that the fractal transformation successfully enriches the phase space structure, transforming a single-scroll attractor into a geometrically complex multi-wing configuration while preserving the chaotic nature of the dynamics.

## 5 Multi-wing chaotic systems generated by modified Julia fractal with coefficient

Now we consider multiplying the term $Z_n^2$ in the Julia fractal expression $Z_{n+1} = Z_n^2 + Z_0$ by a coefficient $k$, obtaining the modified Julia fractal [15]:

$$Z_{n+1} = kZ_n^2 + Z_0. \tag{21}$$

In this case, the mapping matrix takes the form:

$$Df_k = \begin{bmatrix} \frac{\partial u}{\partial x} & \frac{\partial u}{\partial y} & \frac{\partial u}{\partial z} \\ \frac{\partial v}{\partial x} & \frac{\partial v}{\partial y} & \frac{\partial v}{\partial z} \\ \frac{\partial w}{\partial x} & \frac{\partial w}{\partial y} & \frac{\partial w}{\partial z} \end{bmatrix} = \begin{bmatrix} 2kx & -2ky & 0 \\ 2ky & 2kx & 0 \\ 0 & 0 & 1 \end{bmatrix}.$$

(22)
The inverse Jacobian becomes:

$$Df_k^{-1} = \frac{1}{2k(x^2+y^2)} \begin{bmatrix} x & y & 0 \\ -y & x & 0 \\ 0 & 0 & 2k(x^2+y^2) \end{bmatrix}.$$

(23)
Using the same method as in the previous section, and applying the transformation $u = k(x^2 - y^2)$, $v = 2kxy$, $w = z$ to system (1), we obtain the modified multi-wing chaotic system:

$$\begin{cases} \dot{x} = \frac{x}{2k(x^2+y^2)} \left[a(-k(x^2-y^2) + 2kxy)\right] + \\ +\frac{y}{2k(x^2+y^2)} \left[-z \tanh(k(x^2-y^2))\right], \\ \dot{y} = \frac{-y}{2k(x^2+y^2)} \left[a(-k(x^2-y^2) + 2kxy)\right] + \\ +\frac{x}{2k(x^2+y^2)} \left[-z \tanh(k(x^2-y^2))\right], \\ \dot{z} = |k(x^2-y^2)| - 1. \end{cases}$$

(24)

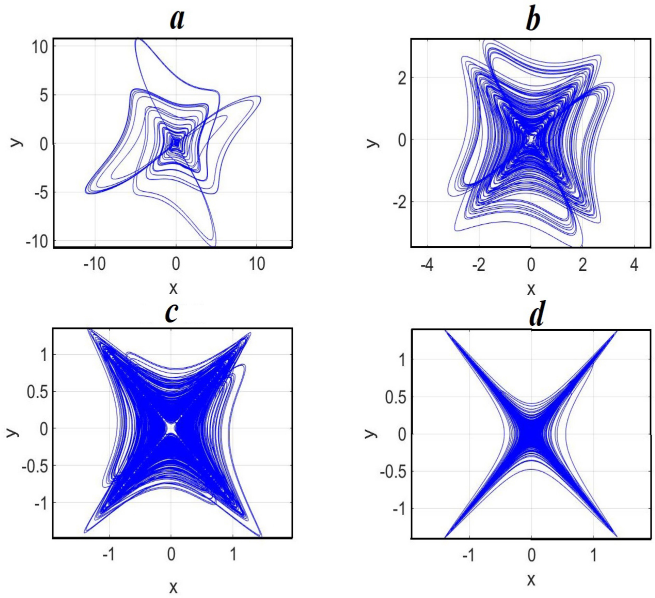


Figure 7: Chaotic attractors of system (25) in the $x$-$y$ plane for different values of parameter $k$: (a) $k = 0.1$; (b) $k = 1.0$; (c) $k = 10.0$; (d) $k = 100.0$.

Simplifying by canceling the coefficient $k$ in the numerator and denominator:

$$\begin{cases} \dot{x} = \frac{x}{2(x^2+y^2)} \left[a(-(x^2-y^2) + 2xy)\right] + \\ +\frac{y}{2(x^2+y^2)} \left[-z \tanh(k(x^2-y^2))\right], \\ \dot{y} = \frac{-y}{2(x^2+y^2)} \left[a(-(x^2-y^2) + 2xy)\right] + \\ +\frac{x}{2(x^2+y^2)} \left[-z \tanh(k(x^2-y^2))\right], \\ \dot{z} = k|x^2-y^2| - 1. \end{cases} \tag{25}$$

Fig. 7 demonstrates the phase space projections of system (25) in the $x$-$y$ plane for parameter $a = 0.55$ and various values of the scaling coefficient $k$. The analysis reveals a systematic geometric transformation of the multi-wing attractor structure as $k$ varies across multiple orders of magnitude. For $k = 0.1$, the attractor exhibits a spatially extended configuration spanning approximately $x, y \in [-15, 15]$. The four-wing butterfly structure remains recognizable but appears distorted and asymmetric, with one wing extending significantly further than the others. This asymmetry suggests that small values of $k$ weaken the constraining effect of the nonlinear terms, allowing trajectories to explore larger regions of phase space before being folded back toward the central manifold. The relatively sparse distribution of trajectories indicates that the chaotic dynamics operate on a much larger spatial scale compared to higher $k$ values. At $k = 1.0$, the canonical four-wing structure emerges with optimal geometric balance and symmetry. The attractor occupies the region $x, y \in [-4, 4]$ and displays the characteristic butterfly morphology with four well-defined lobes arranged symmetrically about the origin. The trajectory density is substantially higher than at $k = 0.1$, indicating that orbits are more tightly confined within the attractor's basin. This configuration represents the natural scaling of system (25) where the fractal transformation preserves the essential topological features of the original system (1) while generating the multi-wing structure through the quadratic mapping. As $k$ increases to 10.0, a dramatic compression of the attractor occurs, with the phase space extent reduced to approximately $x, y \in [-2, 2]$. The four-wing structure becomes significantly more compact and densely packed. The wings retain their fundamental shape but appear thicker and more concentrated, with trajectories forming multiple layers that create a visually solid appearance in the central region. This compression demonstrates that larger $k$ values strengthen the nonlinear coupling through both the $\tanh(k(x^2-y^2))$ term and the modified $z$-dynamics, creating stronger restoring forces that confine trajectories to a smaller spatial domain. At the extreme value $k = 100.0$, the attractor undergoes maximal compression, occupying only $x, y \in [-2, 2]$. The four-wing topology is still preserved, but the structure appears almost perfectly symmetric and highly concentrated. The individual wings become sharply defined with smooth, nearly linear boundaries, and the central region exhibits extremely high trajectory density. The attractor resembles a tightly wound cross or star pattern, where the chaotic dynamics are compressed into a minimal spatial volume while maintaining topological complexity. The saturation of the tanh function at large arguments ($k(x^2 - y^2)$) contributes to this regularization, as the nonlinear term effectively becomes a sign function, creating piecewise-linear dynamics in different regions of phase space.

This systematic scaling behavior reveals that the coefficient $k$ functions as a geometric control parameter that modulates the spatial extent of the chaotic attractor without fundamentally altering its topological structure.

# 6 Multi-wing chaotic systems generated by high-order Julia fractal

Starting from the classical Julia iteration

$$Z_{n+1} = Z_n^2 + Z_0, \tag{26}$$

we replace the quadratic term $Z_n^2$ by a higher-order power $Z_n^m$ and obtain the generalized high-order Julia fractal [14, 15]:

$$Z_{n+1} = Z_n^m + Z_0, \quad m \in \mathbb{N}^+. \tag{27}$$

For $m > 2$, this complex mapping can be embedded into the continuous-time framework of Section 4 by introducing the transformation

$$u + iv = (x + iy)^m, \qquad w = z,$$

that is,

$$u = \Re[(x + iy)^m], \qquad v = \Im[(x + iy)^m].$$

Under this transformation, the state vector $(x, y, z)$ is mapped to $(u, v, w)$, and the dynamics of the original chaotic system are reconstructed in the new coordinates.

Applying the inverse Jacobian of the mapping $(x, y) \mapsto (u, v)$, the resulting multi-wing chaotic system takes the form

$$\begin{bmatrix} \dot{x} \\ \dot{y} \\ \dot{z} \end{bmatrix} = \begin{bmatrix} \frac{S_{m-1}}{m|x+iy|^{2m-2}} & -\frac{T_{m-1}}{m|x+iy|^{2m-2}} & 0 \\ \frac{T_{m-1}}{m|x+iy|^{2m-2}} & \frac{S_{m-1}}{m|x+iy|^{2m-2}} & 0 \\ 0 & 0 & 1 \end{bmatrix} \begin{bmatrix} a(-u+v) \\ -w \tanh u \\ |u| - 1 \end{bmatrix}, \tag{28}$$

where the matrix represents the inverse Jacobian of the polynomial mapping $(x, y) \mapsto (u, v)$ and ensures that the flow of the original system in $(u, v, w)$ is consistently transferred back to the $(x, y, z)$ coordinate space.

The coefficients $S_{m-1}$ and $T_{m-1}$ are defined as the real and imaginary parts of $(x + iy)^{m-1}$:

$$S_{m-1} = \Re[(x+iy)^{m-1}] = \\ = \begin{cases} x^{m-1} + \displaystyle\sum_{l=1}^{(m-2)/2} (-1)^l \binom{m-1}{2l} x^{m-2l-1} y^{2l}, & m \text{ even}, \\ x^{m-1} + \displaystyle\sum_{l=1}^{(m-1)/2} (-1)^l \binom{m-1}{2l} x^{m-2l-1} y^{2l}, & m \text{ odd}, \end{cases} \tag{29}$$

$$T_{m-1} = \Im[(x+iy)^{m-1}] = \\ = \begin{cases} \displaystyle\sum_{l=1}^{m/2} (-1)^{l-1} \binom{m-1}{2l-1} x^{m-2l} y^{2l-1}, & m \text{ even}, \\ \displaystyle\sum_{l=1}^{(m-1)/2} (-1)^{l-1} \binom{m-1}{2l-1} x^{m-2l} y^{2l-1}, & m \text{ odd}. \end{cases} \tag{30}$$

Similarly, the explicit expressions for $u$ and $v$ are given by

$$u = \Re[(x+iy)^m] = \\ = \begin{cases} x^m + \displaystyle\sum_{l=1}^{m/2} (-1)^l \binom{m}{2l} x^{m-2l} y^{2l}, & m \text{ even}, \\ x^m + \displaystyle\sum_{l=1}^{(m-1)/2} (-1)^l \binom{m}{2l} x^{m-2l} y^{2l}, & m \text{ odd}, \end{cases} \tag{31}$$

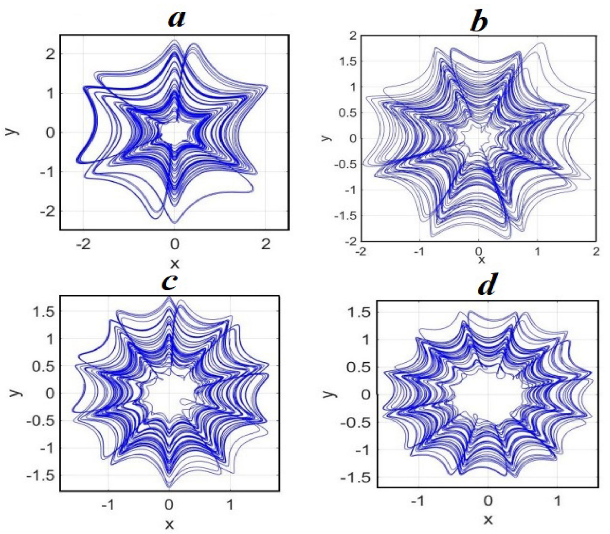

Figure 8: Attractors of a multi-wing chaotic system: (a) $m = 3$ (6-wing chaotic system); (b) $m = 4$ (8-wing chaotic system); (c) $m = 5$ (10-wing chaotic system); (d) $m = 6$ (12-wing chaotic system).

$$v = \Im[(x+iy)^m] =$$
$$= \begin{cases} \displaystyle\sum_{l=1}^{m/2}(-1)^{l+1}\binom{m}{2l-1}x^{m-2l+1}y^{2l-1}, & m \text{ even}, \\ \displaystyle\sum_{l=1}^{(m+1)/2}(-1)^{l+1}\binom{m}{2l-1}x^{m-2l+1}y^{2l-1}, & m \text{ odd}. \end{cases} \tag{32}$$

Extensive numerical simulations indicate that for any integer $m > 1$, system (28) produces a multi-wing chaotic attractor. Fig. 8 illustrates the projections of these attractors onto the $x$-$y$ plane for $a = 0.55$ and $m = 3, 4, 5, 6$, respectively.

A remarkable scaling law is revealed by the high-order Julia transformation: the number of wings in the attractor is equal to $2m$. Specifically, for $m = 3$ a six-wing attractor with three-fold rotational symmetry is obtained; for $m = 4$ an eight-wing structure with four-fold symmetry emerges; for $m = 5$ the attractor develops ten wings; and for $m = 6$ a highly intricate twelve-wing configuration is produced.

As $m$ increases, the wings become more numerous and more densely distributed around the origin, while preserving the global radial symmetry inherited from the complex polynomial mapping $(x+iy)^m$. This demonstrates that the high-order Julia fractal transformation provides a systematic and flexible mechanism for controlling the topological complexity of chaotic attractors through a single integer parameter $m$.

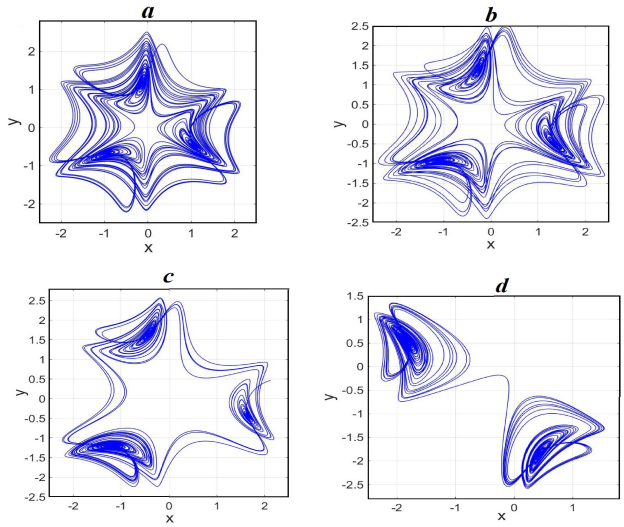

Figure 9: Transformation of the multi-wing chaotic attractor in the $x$-$y$ plane for $m = 3$ at different values of the complex constant $Z_0$: (a) $Z_0 = -0.5 + i1.5$; (b) $Z_0 = -1.5 + i2.5$; (c) $Z_0 = -3.5 + i3.5$; (d) $Z_0 = 4.4 - i5.5$.

# 7 Influence of a nonzero complex constant

In the previous analysis, the complex constant in the generalized Julia mapping was assumed to be zero, which leads to a symmetric polynomial transformation of the form

$$u + iv = (x+iy)^m.$$

In this subsection, we investigate the effect of introducing a nonzero complex constant [15]:

$$Z_0 = x_0 + iy_0 \neq 0$$

into the transformation,

$$u + iv = (x+iy)^m + Z_0. \tag{33}$$

Since $Z_0$ is an additive constant, the Jacobian matrix of the mapping and its inverse remain unchanged. Therefore, the local stretching and folding mechanism responsible for the generation of multi-wing chaotic attractors is preserved. The role of $Z_0$ is to shift the image of the polynomial mapping in the complex plane, which results in a deformation of the global geometry of the attractor. Numerical simulations show that a nonzero $Z_0$ breaks the exact rotational symmetry of the $2m$-wing structure obtained for $Z_0 = 0$. Depending on the magnitude and phase of $Z_0$, the wings become asymmetric and unequally distributed around the origin, while the total number of wings remains unchanged. This indicates that the complex constant acts as a deformation parameter controlling the spatial arrangement of the wings rather than their number.

Fig. 9 illustrates the topological transformation of the multi-wing chaotic attractor as the complex constant $Z_0$ varies. For $Z_0 = -0.5 + i1.5$ (Fig. 9a), the system exhibits a symmetric six-wing attractor with uniform distribution of trajectories. As $Z_0$ changes to $Z_0 = -1.5 + i2.5$ and $Z_0 = -3.5 + i3.5$ (Fig. 9b and Fig. 9c), progressive symmetry breaking occurs, with trajectories redistributing among the wings. A dramatic topological change is observed at $Z_0 = 4.4 - i5.5$ (Fig. 9d), where the attractor collapses into an asymmetric two-wing structure. This demonstrates the structural sensitivity of multi-wing attractors to parameter variations and reveals how $Z_0$ acts as a bifurcation parameter controlling the attractor's morphology.

### 7.1 Perspectives on the application of Mandelbrot iterations

The Mandelbrot iteration process $Z_{n+1} = Z_n^2 + c$, where $c$ is a fixed complex constant and $Z_0 = 0$, is structurally similar to the Julia transformation employed in this work. The key distinction lies in the role of the control parameter: in the case of the Julia set, the value of $c$ is fixed while the initial condition $Z_0$ varies across the phase space. In the Mandelbrot approach, conversely, the parameter $c$ itself is varied for a fixed $Z_0 = 0$, which yields a different parametric dependence for the attractor morphology. This opens the possibility of generating attractors with an irregular distribution of ”wings” that lack the strict $2m$-fold rotational symmetry characteristic of the standard Julia transformation.

## 8 Conclusion

In this paper, we have introduced a novel three-dimensional chaotic system combining hyperbolic tangent and absolute value nonlinearities. Despite its minimal algebraic complexity with only five terms, the system exhibits rich chaotic dynamics with a positive Lyapunov exponent $LE_1 = 0.12790$ and Kaplan-Yorke dimension $D_{KY} \approx 2.206$. The system possesses two unstable saddle-focus equilibrium points and generates a symmetric two-wing attractor. The principal contribution of this work is the systematic application of the Julia fractal process to generate multi-wing chaotic attractors. By introducing the polynomial transformation $u + iv = (x + iy)^m$ derived from the generalized Julia iteration $Z_{n+1} = Z_n^m + Z_0$, we developed a framework that enriches the phase space topology while preserving chaotic properties. Numerical simulations revealed a remarkable scaling law: the number of wings equals $2m$, where $m$ is the polynomial order. The classical transformation ($m = 2$) produces a four-wing attractor, while higher orders generate six, eight, ten, and twelve wings for $m = 3, 4, 5, 6$, respectively. The scaling coefficient $k$ provides geometric control over attractor size without altering topology, and the complex constant $Z_0$ enables asymmetric wing configurations while preserving wing number. The proposed methodology offers several advantages: smooth analytical transformations avoiding piecewise discontinuities, explicit control through parameters $m$, $k$, and $Z_0$, and preservation of chaotic dynamics. The minimal structure and combination of tanh and absolute value functions facilitate hardware implementation for secure communications and chaotic encryption applications.

Future research directions include experimental circuit validation, investigation of synchronization properties for secure communications, extension to higher-dimensional and memristive systems, and exploration of alternative fractal processes such as the Mandelbrot fractal for generating novel attractor topologies.

*References:*

[1] E. N. Lorenz: Deterministic nonperiodic flow. *Journal of atmospheric sciences*, **20**(2) (1963), 130-141. https://doi.org/10.1175/1520-0469(1963)020<0130:DNF>2.0.CO;2

[2] O. E. Rössler: An equation for continuous chaos. *Physics Letters A*, **57**(5) (1976), 397-398. https://doi.org/10.1016/0375-9601(76)90101-8

[3] L. O. Chua, M. Komuro, T. Matsumoto: The double scroll family. *IEEE Transactions on Circuits and Systems*, **33**(11) (1986), 1072-1118. https://doi.org/10.1109/TCS.1986.1085869

[4] K. Benkouider et al.: Dynamics, Control and Secure Transmission Electronic Circuit Implementation of a New 3D Chaotic System in Comparison With 50 Reported Systems. *IEEE Access*, **9** (2021) , 152150-152168. https://doi.org/10.1109/ACCESS.2021.3126655

[5] A. Sambas et al.: A Novel 3D Chaotic System With Line Equilibrium: Multistability, Integral Sliding Mode Control, Electronic Circuit, FPGA Implementation and Its Image Encryption. *IEEE Access*, **10** (2022), 68057-68074. https://doi.org/10.1109/ACCESS.2022.3181424

[6] J. Wang, C. Dong, H. Li: A New Variable-Boostable 3D Chaotic System with Hidden and Coexisting Attractors: Dynamical Analysis, Periodic Orbit Coding, Circuit Simulation, and Synchronization. *Fractal Fract.*, **6** (2022), 740. https://doi.org/10.3390/fractalfract6120740

[7] Ali A. Shukur, Ammar Ali Neamah, Viet-Thanh Pham, Giuseppe Grassi: A novel chaotic system with one absolute term: stability, ultimate boundedness, and image encryption *Heliyon*, **11** (2025), e37239. https://doi.org/10.1016/j.heliyon.2024.e37239

[8] M.D. Johansyah et al.: Exploring Chaos and Stability in a 3-D Finance Model with Absolute Function Nonlinearity. *Mathematics*, **13** (2025), 735. https://doi.org/10.3390/math13050735

[9] S. Shi, H. Lu, C. Du, Z. Zhang, L. Liu: Analysis and application of a 3D chaotic system with an extremely extensive range of amplitudes and offset boosting. *Phys. Scr.*, **100** (2025), 025209. https://doi.org/10.1088/1402-4896/ada11b

[10] S. Kosmidis, C. Volos, L. Moysis, E. Meletlidou: A Novel Chaotic System with Hyperbolic Tangent Terms and Its Application to Random Bit Generator and Image Encryption. *Journal of Vibration Testing and System Dynamics*, **1**(1) (2017), 1-6. https://doi.org/10.5890/JVTSD.2017.03.001

[11] Fei Yu et al.: A new multi-scroll Chua's circuit with composite hyperbolic tangent-cubic nonlinearity: Complex dynamics, Hardware implementation and Image encryption application. *Integration*, **81**(10) (2021), 71-83. https://doi.org/10.1016/j.vlsi.2021.05.011

[12] A. S. Elwakil, S. Ozoguz, M. P. Kennedy: Creation of a complex butterfly attractor using a novel Lorenz-Type system. *IEEE Transactions on Circuits and Systems I: Fundamental Theory and Applications*, **49**(4) (2002), 527-530. https://doi.org/10.1109/81.995671

[13] V. K. Tamba, K. Rajagopal, V.-T. Pham, D. V. Hoang: Chaos in a System with an Absolute Nonlinearity and Chaos Synchronization. *Advances in Mathematical Physics*, **2018** (2018), Article ID 5985489, 12 pages. https://doi.org/10.1155/2018/5985489

[14] Y. Guo, G. Qi, Y. Hamam: A multi-wing spherical chaotic system using fractal process. *Nonlinear Dynamics*, (2016). https://doi.org/10.1007/s11071-016-2861-7

[15] L. Q. Xiao, S. K. Duan, and L. D. Wang: Julia fractal based multi-scroll memristive chaotic system. *Acta Physica Sinica*, **67** (2018), 090502. https://doi.org/10.7498/aps.67.20172761.

[16] D. Yan, E. Ji, L. Wang, and S. Duan: Generating novel multi-scroll chaotic attractors via fractal transformation. *Nonlinear Dynamics*, **110**(3) (2022), 2669-2689. https://doi.org/10.1007/s11071-022-07738-1.

[17] M. I. Kopp: Generation of multi-scroll attractors in a new 4D memristor-based hyperchaotic system using fractal transformations: from simulation to microcontroller design. TechRxiv. December 08, 2025. https://doi.org/10.36227/techrxiv.176522719.95864495/v1

[18] G. Benettin, L. Galgani, A. Giorgilli, J.-M. Strelcyn: Lyapunov characteristic exponents for smooth dynamical systems and for Hamiltonian systems: A method for computing all of them. *Meccanica*, **15** (1980), 9-20.

[19] H. Binous, N. Zakia. An Improved Method for Lyapunov Exponents Computation. https://library.wolfram.com/infocenter/MathSource/7109/, March 09, 2008.

[20] M. Sandri: Numerical Calculation of Lyapunov Exponents. *Mathematica J.*, **6** (1996), 78-84. https://library.wolfram.com/infocenter/Articles/2902/

[21] E. W. Weisstein: *Routh-Hurwitz Theorem*. From MathWorld – A Wolfram Web Resource. https://mathworld.wolfram.com/Routh-HurwitzTheorem.html

[22] G. A. Gottwald and I. Melbourne: A new test for chaos in deterministic systems. *Proceedings of the Royal Society of London A*, **460** (2004), 603–611. https://doi.org/10.1098/rspa.2003.1183

[23] G. A. Gottwald and I. Melbourne: Testing for chaos in deterministic systems with noise. *Physica D: Nonlinear Phenomena*, **212** (2005), 100–110. https://doi.org/10.1016/j.physd.2005.09.011

**Contribution of Individual Authors to the Creation of a Scientific Article (Ghostwriting Policy)**

The authors equally contributed in the present research, at all stages from the formulation of the problem to the final findings and solution.

**Sources of Funding for Research Presented in a Scientific Article or Scientific Article Itself**

No funding was received for conducting this study.

**Conflict of Interest**

The authors have no conflicts of interest to declare that are relevant to the content of this article.